NJC

COMMUNICATION

View Article Online
View Journal | View Issue

Cite this: *New J. Chem.*, 2024, **48**, 15281

Received 21st June 2024,
Accepted 8th August 2024

DOI: 10.1039/d4nj02834a

rsc.li/njc

A nonlinear optical crystal with deep-ultraviolet transparency and appropriate birefringence achieved using π-conjugated confined $[B_3O_3F_4(OH)]^{2-}$†

Tao Ouyang,[ab] Xu Chen,[ab] Shanshan Chen,[b] Yanqiang Li,[b] Xiaoying Shang,*[b] Zhiyong Bai,[b] Ningtao Jiang,[c] Zhishuo Yan,[c] Junhua Luo[b] and Sangen Zhao *[b]

Finding a deep-ultraviolet (deep-UV, $\lambda < 200$ nm) nonlinear optical (NLO) crystal is vital to a number of advanced optical technologies, yet it remains a great challenge. Herein, we report a deep-UV NLO crystal, $K_2B_3O_3F_4(OH)$ (KBOFH), composed of π-conjugated confined groups. It exhibits a relatively large birefringence of 0.054@550 nm and a wide transparency window with an absorption edge below 200 nm. Theoretical calculations reveal that the observed optical properties of KBOFH originate from the confined π-conjugated $[B_3O_3F_4(OH)]$ unit, in which the π-conjugated interactions are decoupled by the tetrahedral non-π-conjugated $[BO_2F_2]$ unit. This work provides an opportunity to design deep-UV NLO crystals containing π-conjugated confined groups.

Introduction

Deep-ultraviolet (deep-UV) nonlinear optical (NLO) materials are of tremendous interest owing to their ability to generate deep-UV coherent light from common lasers (*e.g.*, Nd:YAG 1064 nm, infrared) by a cascade frequency-doubling process.[1–5] The prerequisites essential for deep-UV NLO crystals include (1) large second harmonic generation (SHG) efficiency, (2) a wide transmittance range down to below 200 nm, (3) suitable birefringence to phase match, (4) high laser-induced damage threshold (LIDT), and (5) good physiochemical properties, among others.[6–16] In this context, borate lies in one of the most promising and investigated material systems for deep-UV NLO.[17–27] Nevertheless, it is still very difficult to develop efficient deep-UV NLO borates as their performance criteria are generally mutually exclusive in the deep-UV region. Against this background, intense efforts have been made to develop borates.[28–35]

Conventional borates are generally composed of π-conjugated $[BO_3]$ with sp^2-hybridization and (or) non π-conjugated $[BO_4]$ with sp^3-hybridization. It is found that compared to the planar $[BO_3]$ unit, tetrahedral $[BO_4]$ shows much lower hyperpolarizability, polarizability anisotropy, resulting in unsatisfactory NLO properties, such as subpar birefringence. Pan's group discovered that the fluorinated $[BO_xF_{4-x}]$ (x = 1–3) units are able to exhibit larger polarizability anisotropy and hyperpolarizability than the $[BO_4]$ unit,[36] and are thus considered to be attractive functional building blocks (FBBs) to synthesize deep-UV NLO materials. On the other hand, the π-conjugated $[BO_3]$ unit is the most attractive FBB for the design of deep-UV NLO materials; however, its dangling bonds have a negative impact on the band gap.

Recently, Chen's group has put forward a so-called π-conjugated confinement concept which refers to restriction of π-conjugated by non-π-conjugated groups to reduce π-conjugated interactions between the units, thereby broadening the bandgap while retaining the desired birefringence. Guided by this proposal, the carbonophosphate $Sr_3Y[PO_4][CO_3]_3$ exhibits a combination of an appropriate birefringence value of 0.121@532 nm and a wide bandgap value of 6.9 eV.[37] In $Sr_3Y[PO_4][CO_3]_3$, π-conjugated $[CO_3]$ and non π-conjugated $[PO_4]$ are not directly linked. We think that the confinement effect can probably be enhanced when the π-conjugated unit and the non π-conjugated unit are directly bridged by covalent bonds since such direct connections can eliminate the dangling bonds of π-conjugated groups more effectively, thereby giving rise to enlarged band gaps while not compromising on the optical anisotropy too much. With these in mind, we endeavour to combine the π-conjugated $[BO_3]$ with the non-π-conjugated $[BO_xF_{4-x}]$ (x = 1–3) units by taking the known

[a] *College of Chemistry, Fuzhou University, Fuzhou 350116, China*
[b] *State Key Laboratory of Structural Chemistry, Fujian Institute of Research on the Structure of Matter, Chinese Academy of Sciences, Fuzhou 350002, China. E-mail: shangxiaoying@fjirsm.ac.cn, zhaosangen@fjirsm.ac.cn*
[c] *Department of Electrical and Computer Engineering, North Dakota State University, Fargo 58102, USA*

† Electronic supplementary information (ESI) available: Crystallographic data, atomic coordinates and equivalent isotropic displacement parameters, anisotropic displacement parameters, selected bond lengths and angles tables, powder XRD pattern, EDS data, UV-vis-NIR spectra, TG and DTA data, FTIR data, the thickness of the selected KBOFH single-crystal used for the birefringence measurement and refractive index dispersion curves are given. CCDC 2353235. For ESI and crystallographic data in CIF or other electronic format see DOI: https://doi.org/10.1039/d4nj02834a

$[B_3O_6]^{3-}$ as a parent to construct new deep-UV NLO crystals. By doing so, a noncentrosymmetric (NCS) fluoroborate (KBOFH) has been successfully synthesized. In the structure, a π-conjugated confined $[B_3O_3F_4OH]^{2-}$ FBB is identified, which is composed of one π-conjugated planar $[BO_2(OH)]$ group and two non π-conjugated $[BO_2F_2]$ tetrahedrons by corner-sharing. In this work, we report its synthesis, crystal structure, and NLO properties, and investigate the underlying mechanisms of optical properties by a theoretical approach.

Experimental section

Single crystals of KBOFH were synthesized *via* a hydrothermal method. Triethylamine serves as both a solvent and a mineralizer. Typically, $La(NO_3)_3{\cdot}6H_2O$ (Adamas, 99.9%, 0.9 mmol, 0.389 g), KBF_4 (Aladdin, 99.0%, 2.7 mmol, 0.34 g), B_2O_3 (Aladdin, 99.0%, 1.2 mmol, 0.084 g), triethylamine (Greagent, > 99.0%, 2 mL) and deionized water (1 mL) were combined into a 23 mL Teflon-lined Parr autoclave and mixed well. The mixture was heated to 200 °C, held for 5000 min, and then cooled to 30 °C within 2000 min. Colourless transparent laminar crystals were harvested.

Results

Crystal structure

The purity of the synthesized KBOFH which was washed several times with acetone has been examined using powder X-ray diffraction (PXRD) (Fig. S1, ESI†). To examine the stability in air, KBOFH was exposed to air for one week. As displayed in Fig. S2 (ESI†), the surface of the exposed crystal is nearly unchanged. A further PXRD test of the exposed KBOFH showed a good match with the original PXRD patterns (Fig. S3, ESI†). These results indicate that KBOFH is stable in air. The mapping of elemental scanning electron microscopy (SEM) analysis revealed the existence of elements K, B, O, and F in KBOFH (Fig. 1a), which were also confirmed by energy-dispersive X-ray spectroscopy (EDX) (Fig. S4, ESI†). As shown in Fig. S4 (ESI†), the molar ratio of O to F in KBOFH is close to 1.

KBOFH crystallizes in the NCS space group *Ama*2 (No. 40) with orthorhombic cell parameters of a = 25.9308(5) Å, b = 22.5853(4) Å, c = 7.46320(10) Å, Z = 24, and V = 4370.86(13) Å^3 (see details in Tables S1–S5, ESI†). The asymmetric unit consists of 12 independent B atoms, 13 F atoms, 16 O atoms, and 7 K atoms. B3, B6, and B9 exhibit a triangular $[BO_2(OH)]$ configuration while B1, B2, B4, B5, B7, B8, B10, and B11 are bonded to two O atoms and two F atoms to form $[BO_2F_2]$ tetrahedrons. The bond lengths and bond angles within $[BO_2(OH)]$ and $[BO_2F_2]$ are listed in Tables S4 and S5 (ESI†), which are comparable to previously reported compounds, such as $Rb_2B_3O_3F_4(OH)$[38] and $Cs_2B_3O_3F_4(OH)$.[39] Its structure consists of isolated three-membered rings $[B_3O_3F_4OH]^{2-}$ composed of a π-conjugated planar $[BO_2(OH)]$ group and two non π-conjugated $[BO_2F_2]$ tetrahedrons by corner-sharing. The $[B_3O_3F_4OH]^{2-}$ units are further connected by hydrogen bonding, resulting in one-dimensional chains (Fig. 1b). These chains are linked by K atoms to form a three-dimensional structure (Fig. 1c).

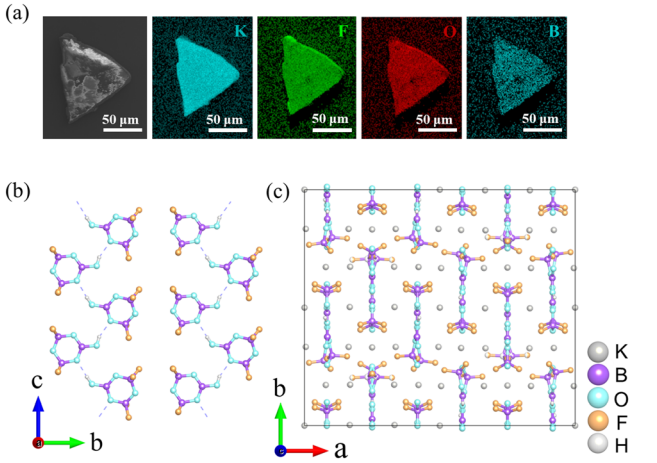

Fig. 1 Elemental analysis and crystal structure of KBOFH. (a) Scanning electron microscope elemental mapping. The structure of KBOFH is viewed along the (b) *a* axis and (c) *c* axis.

The $[B_3O_3F_4OH]^{2-}$ rings are nearly parallel to each other which might facilitate large optical anisotropy for KBOFH.

The UV-vis-NIR diffuse reflectance spectrum of KBOFH was collected in the wavelength range of 200–1000 nm (Fig. S5, ESI†). A relatively high reflectance of *ca.* 60% at 200 nm was observed, revealing that KBOFH is deep-UV transparent and has a band gap larger than 6.2 eV.

The infrared spectroscopy (FTIR) spectrum of KBOFH is shown in Fig. S7 in the ESI.† The stretching vibration of O–H can be observed in the range of 3400–3300 cm^{-1}. The absorption signals at about 1420 cm^{-1} and 1039 cm^{-1} correspond to asymmetrical vibration and symmetrical vibration of BO_3. In addition, the sharp absorption signal at about 703 cm^{-1} corresponds to the torsional vibration of BO_3. Furthermore, a significant signal observed at about 844 cm^{-1} is assigned to B–F symmetrical vibration.[40,41]

The powder SHG efficiency of KBOFH was measured at 1064 nm using the Kurtz–Perry method.[42] As shown in Fig. 2a, KBOFH shows a SHG efficiency of *ca.* 0.2 × KDP in the particle size range of 74–124 μm. Furthermore, the SHG intensities continuously raise with the increase of crystal size, indicating that KBOFH is type-I phase-matchable at 1064 nm (Fig. 2b). The relatively weak SHG response exhibited by KBOFH could be attributed to the opposite arrangements of $[B_3O_3F_4OH]^{2-}$ units which offset their dipole moments. These structural arrangements are not preferable for the origination of a large NLO response based on anionic group theory.[43] Fig. 2c presents the SHG response of KBOFH at various excitation wavelengths ranging from 800 to 920 nm, revealing that KBOFH is able to generate SHG output at 400 nm to 460 nm, which further verified the phase-matching ability of KBOFH at 1064 nm. Fig. 2d shows that the SHG intensity of KBOFH increases with the input power, and the inset displays the SHG intensities in logarithmic coordinates as a function of excitation power. The slope of the fitting curve is found to be 2.2, which is in line with the theoretical value of 2, indicating that the collected signals indeed stem from the SHG. Fig. 2e and f display two and four asymmetric lobes respectively,

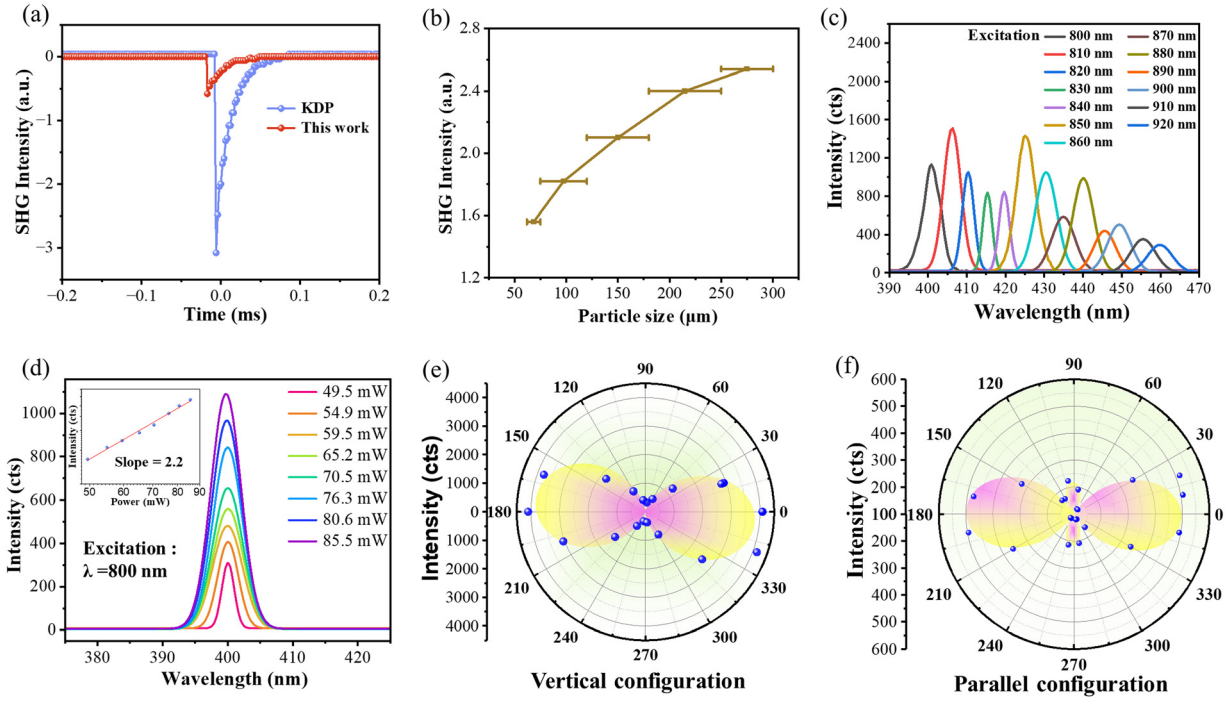

Fig. 2 The second-order nonlinear optical properties of KBOFH. (a) SHG signals of KBOFH and KDP in the particle size range of 74–124 μm. (b) Particle size-dependent SHG responses. The curve is drawn to guide the eyes and not fitted to the data. (c) SHG spectra of a (010) flake of KBOFH at various excitation wavelengths ranging from 800 to 920 nm. (d) Pump power-dependent SHG response in the incident light at 800 nm. Inset: The SHG intensities in logarithmic coordinates as a function of excitation power. Polarization-dependent SHG for (e) vertical configuration and (f) parallel configuration.

resulting from the space group *Ama*2 of KBOFH crystals, suggesting that an in-plane anisotropy existed in the (010) plane of KBOFH.

The birefringence of KBOFH was measured on a polarizing microscope. A schematic diagram illustrating birefringence measurement by polarizing microscope is shown in Fig. 3a. Generally, when polarized light enters the crystal, birefringence occurs and splits the incident light into an ordinary ray (*o* light) and an extraordinary ray (*e* light). The retardation (*R*) occurs between the *o* light and *e* light in this process. Hence, the

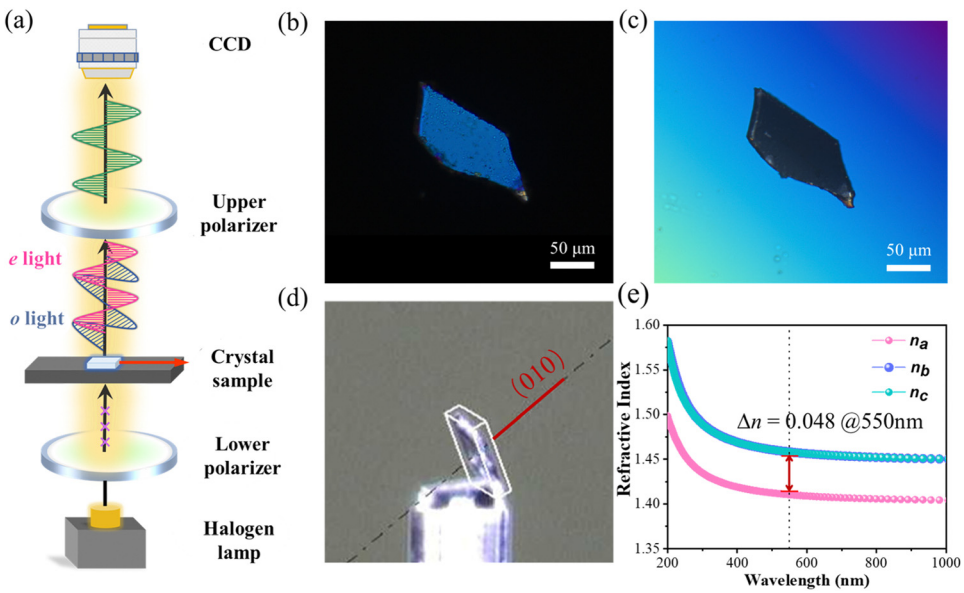

Fig. 3 Birefringence properties of KBOFH. (a) A schematic diagram illustrates the birefringence measurement principle using a polarizing microscope. (b) Original interference of the KBOFH crystal under orthogonally polarized light. (c) KBOFH crystal realizing complete extinction. (d) The orientation of the KBOFH plate used for measurement. (e) Theoretically calculated refractive index dispersion curves of KBOFH.

determination R and the thickness of the crystal plate enable us to measure the birefringence. A selected single crystal of KBOFH exhibits original interference color as blue under orthogonally polarized light (Fig. 3b), which then turns black when a Berek compensator (Fig. 3c), suggesting that extinction has been achieved for measured crystals. At a wavelength of 550 nm, the R-value is determined to be 625 nm, and the measured thickness is 11.53 μm (Fig. S8, ESI†). The orientation of the crystal used for birefringence determination is found to be the (010) plane by SCXRD (Fig. 3d). Based on these results, the birefringence of KBOFH is observed to be $\Delta n_{(010)\mathrm{exp}}$ = 0.054@550 nm in the (010) plane. In addition, based on first-principles calculations,[44] the static refractive indices of KBOFH are found to be n_a = 1.410, n_b = 1.458, and n_c = 1.458 at 550 nm. The calculated birefringence (0.048@550 nm) in the (010) plane is matched well with the experimental value (Fig. 3e). Inspired by the obvious optical anisotropy of KBOFH, we further examined its SHG phase-matching ability using the calculated refractive indices. As shown in Fig. S9 (ESI†), the shortest phase-matching wavelength of KBOFH is determined to be 235 nm, which is comparable to those of a few known deep-UV NLO crystals, such as LBO (277 nm), CLBO (236 nm), and KDP (258 nm).

First-principles calculations were carried out to reveal the structure–property relationships of KBOFH.[45–47] Fig. 4a shows that KBOFH has a band gap of 7.0 eV, close to the experimental observation. The density of states (DOS) and partial DOS diagram of constituent atoms are present in Fig. 4b. The upper region of the valence band (VB) is mainly composed of O 2p, F 2p and B 2p orbitals. The bottom region of the valence band is occupied by O 2p, H 1s, K 3s and K 3p. As the optical properties of crystals are intimately associated with electronic activities near the Fermi level, we can briefly conclude that the bandgap, birefringence, and second-order NLO properties of KBOFH are mainly determined by anionic $[B_3O_3F_4OH]^{2-}$ groups.

To further visualize the contribution of $[B_3O_3F_4OH]^{2-}$ to the optical properties of KBOFH, the highest occupied molecular orbitals (HOMOs), the lowest unoccupied molecular orbitals (LUMOs), and the electron localization function (ELF) calculations were implemented. The HOMO is largely occupied by the 2p orbitals of oxygen and fluorine atoms (Fig. 4c), whereas the LUMO is dominated by K 3p states (Fig. 4d).

Additionally, the occupied π-orbitals of known $[B_3O_6]^{3-}$ and $[B_3O_3F_4OH]^{2-}$ in KBOFH were computed for a comparison of conjugated interactions between them (Fig. 4e). It is found that the π-electron clouds of the $[B_3O_6]^{3-}$ group are highly delocalized. In the case of the $[B_3O_3F_4OH]^{2-}$ group, only σ-bonds were observed for $[BO_2F_2]$ tetrahedra while the planar $[BO_2(OH)]^{2-}$ is also delocalized. Hence, compared to $[B_3O_6]^{3-}$, the electron clouds exhibited by $[B_3O_3F_4OH]^{2-}$ are partly decoupled by the tetrahedral $[BO_2F_2]$ group; in other words, $[B_3O_3F_4OH]^{2-}$ should be categorized as a confined π-conjugated functional unit. In this context, KBOFH may exhibit a wider band gap, and $[B_3O_3F_4OH]^{2-}$ groups could better balance SHG, deep-UV transparency, and birefringence, the three most important criteria for deep-UV NLO materials. Furthermore, the (100) (in-plane) and (001) (out-of-plane) slices of ELF are presented in Fig. 4f and h. For $[B_3O_3F_4OH]^{2-}$, remarkable discrepancy of electron cloud density between the (100) and (001) orientations is observed, which indicates that $[B_3O_3F_4OH]^{2-}$ is anisotropic and should be responsible for the large optical anisotropy exhibited by KBOFH.

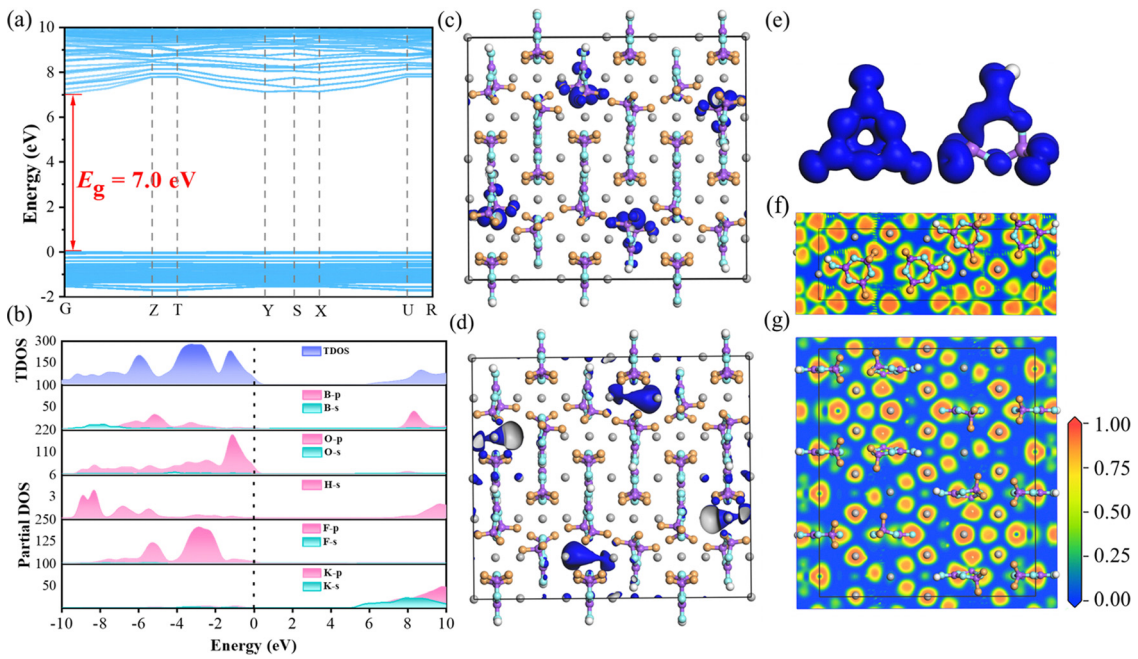

Fig. 4 Theoretical calculations of KBOFH. (a) Electronic band structure. (b) DOS and partial DOS. (c) The HOMO map. (d) The LUMO map. (e) The occupied π bonds in $[B_3O_6]^{3-}$ (left) and $[B_3O_3F_4OH]^{2-}$ (right). (f) (100) (in-plane) projection of the ELF for KBOFH. (g) (001) (out-of-plane) projection of the ELF for KBOFH. The atoms K, B, O, F, and H are denoted using pale grey, purple, pale blue, yellow, and white balls, respectively.

Conclusions

In conclusion, a deep-UV NLO crystal KBOFH has been synthesized *via* a hydrothermal method. KBOFH reveals intriguing NLO properties including a wide band gap of $>$ 6.2 eV and a phase matchable SHG efficiency of *ca.* 0.2 $\times$ KDP. Moreover, its birefringence was measured using a polarizing microscope, revealing that it possesses a relatively large birefringence, Δn_{exp} = 0.054@550 nm, which enables a short phase-matchable limit of 235 nm. The electron localization function (ELF) shows that $[B_3O_3F_4(OH)]^{2-}$ is anisotropic and thus responsible for the large optical anisotropy of KBOFH. The structure–property relationship investigation based on theoretical approaches reveals that the optical properties of KBOFH discussed in this work are mainly determined by the $[B_3O_3F_4OH]^{2-}$ group which is found to be a π-conjugated confined group by HOMO–LUMO analysis.

Author contributions

T. Ouyang performed the main experiments and wrote the paper. X. Chen and S. Chen solved the crystal structure, Y. Li performed the DFT calculations, X. Shang measured the SHG, Z. Bai measured the birefringence, N. Jiang and Z. Yan offered help with data analysis. J. Hua and S. Zhao designed and supervised the overall experiments. All authors discussed and co-wrote the manuscript.

Data availability

In the ESI,† crystallographic data, atomic coordinates and equivalent isotropic displacement parameters, anisotropic displacement parameters, selected bond lengths and angles tables, powder XRD pattern, EDS data, UV-vis-NIR spectra, TG and DTA data, FTIR data, the thickness of the selected KBOFH single-crystal used for the birefringence measurement and refractive index dispersion curves are given.

Conflicts of interest

The authors declare no competing interests.

Acknowledgements

This work acknowledges the financial support from the National Natural Science Foundation of China (22122507, 22193042, and 21921001), the Natural Science Foundation of Fujian Province (2022J02012), the Youth Innovation Promotion Association of Chinese Academy of Sciences (Y202069), and the China Postdoctoral Science Foundation (2023M743498).

References

1 C. Chen, Y. Wang, B. Wu, K. Wu, W. Zeng and L. Yu, Design and Synthesis of an Ultraviolet-Transparent Nonlinear-Optical Crystal $Sr_2Be_2B_2O_7$, *Nature*, 1995, **373**, 322–324.
2 G. Aka, A. KahnHarari, F. Mougel, D. Vivien, F. Salin, P. Coquelin, P. Colin, D. Pelenc and J. P. Damelet, Linear- and Nonlinear-Optical Properties of a New Gadolinium Calcium Oxoborate Crystal, $Ca_4GdO(BO_3)_3$, *J. Opt. Soc. Am. B.*, 1997, **14**, 2238–2247.
3 B. Zhao, B. Li, S. Zhao, X. Liu, Z. Wu, Y. Shen, X. Li, Q. Ding, C. Ji and J. Luo, Physical Properties of a Promising Nonlinear Optical Crystal $K_3Ba_3Li_2Al_4B_6O_{20}F$, *Cryst. Growth Des.*, 2018, **18**, 7368–7372.
4 X. Shi, A. Tudi, M. Cheng, F. Zhang, Z. Yang, S. Han and S. Pan, Noncentrosymmetric Rare-Earth Borate Fluoride $La_2B_5O_9F_3$: A New Ultraviolet Nonlinear Optical Crystal with Enhanced Linear and Nonlinear Performance, *ACS Appl. Mater.*, 2022, **14**, 18704–18712.
5 Y. Song, H. Yu, B. Li, X. Li, Y. Zhou, Y. Li, C. He, G. Zhang, J. Luo and S. Zhao, A Ferroelectric Nonlinear Optical Crystal for Deep-UV Quasi-Phase-Matching, *Adv. Funct. Mater.*, 2024, **34**, 2310407.
6 Y. Shen, J. Jia, Z. Liu, J. Wang, S. Zhao and J. Luo, Structurally Stable Borate as a UV Nonlinear Optical Material, *Inorg. Chem. Commun.*, 2017, **84**, 127–130.
7 P. Becker, Borate Materials in Nonlinear Optics, *Adv. Mater.*, 1998, **10**, 979–992.
8 S. Zhao, J. Zhang, S. Zhang, Z. Sun, Z. Lin, Y. Wu, M. Hong and J. Luo, A New UV Nonlinear Optical Material $CsZn_2B_3O_7$: ZnO_4 Tetrahedra Double the Efficiency of Second-Harmonic Generation, *Inorg. Chem.*, 2014, **53**, 2521–2527.
9 M. Mutailipu, F. Li, C. Jin, Z. Yang, K. R. Poeppelmeier and S. Pan, Strong Nonlinearity Induced by Coaxial Alignment of Polar Chain and Dense $[BO_3]$ Units in $CaZn_2(BO_3)_2$, *Angew. Chem., Int. Ed.*, 2022, **61**, e202202096.
10 C. Chen, B. Wu, A. Jiang and G. You, A New-Type Ultraviolet SHG Crystal—β-BaB_2O_4, *Sci. Sin. B*, 1985, **28**, 235–243.
11 D. Eimerl, L. Davis, S. Velsko, E. K. Graham and A. Zalkin, Optical, Mechanical, and Thermal-Properties of Barium Borate, *J. Appl. Phys.*, 1987, **62**, 1968–1983.
12 P. S. Halasyamani and J. M. Rondinelli, The Must-Have and Nice-to-Have Experimental and Computational Requirements for Functional Frequency Doubling Deep-UV Crystals, *Nat. Commun.*, 2018, 9.
13 C. Chen, N. Ye, J. Lin, J. Jiang, W. Zeng and B. Wu, Computer-Assisted Search for Nonlinear Optical Crystals, *Adv. Mater.*, 1999, **11**, 1071–1078.
14 X. Chen, Y. Li, J. Luo and S. Zhao, Recent Advances in non-π-Conjugated Nonlinear Optical Sulfates with Deep-UV Absorption Edge, *Chin. J. Struct. Chem.*, 2023, **42**, 100044.
15 H. Wang, J. Liu, M. Li, Y. Li, Y. Zhou, W. Liu, J. Luo and S. Zhao, A New 2D van der Waals Material with Air Stability and in-plane Anisotropy, *Chin. J. Struct. Chem.*, 2023, **42**, 100099.
16 Y. Li, Q. Wu, Z. Lin, Y. Liu, Y. Zhou, X. Chen, M. Li, M. Hong, J. Luo and S. Zhao, Maximizing the linear and nonlinear optical responses of alkaline tricyanomelaminate, *Fundam. Res.*, 2023, **3**, 974–978.
17 C. Chen, Y. Wu, A. Jiang, B. Wu, G. You, R. Li and S. Lin, New Nonlinear-Optical Crystal–LiB_3O_5, *J. Opt. Soc. Am. B*, 1989, **6**, 616–621.

18 F. Kong, S. Huang, Z. Sun, J. Mao and W. Cheng, $Se_2(B_2O_7)$: A New Type of Second-Order NLO Material, *J. Am. Chem. Soc.*, 2006, **128**, 7750–7751.
19 H. Huppertz and B. von der Eltz, Multianvil High-Pressure Synthesis of $Dy_4B_6O_{15}$: The First Oxoborate with Edge-Sharing BO_4 Tetrahedra, *J. Am. Chem. Soc.*, 2002, **124**, 9376–9377.
20 G. Zou, C. Lin, H. Jo, G. Nam, T. S. You and K. M. Ok, Pb_2BO_3Cl: A Tailor-Made Polar Lead Borate Chloride with very Strong Second Harmonic Generation, *Angew. Chem., Int. Ed.*, 2016, **55**, 12078–12082.
21 P. Gross, A. Kirchhain and H. A. Höppe, The Borosulfates $K_4[BS_4O_{15}(OH)]$, $Ba[B_2S_3O_{13}]$, and $Gd_2[B_2S_6O_{24}]$, *Angew. Chem., Int. Ed.*, 2016, **55**, 4353–4355.
22 C. Wu, C. Jiang, G. Wei, X. Jiang, Z. Wang, Z. Lin, Z. Huang, M. G. Humphrey and C. Zhang, Toward Large Second-Harmonic Generation and Deep-UV Transparency in Strongly Electropositive Transition Metal Sulfates, *J. Am. Chem. Soc.*, 2023, **145**, 3040–3046.
23 Y. Zhou, X. Zhang, Z. Xiong, X. Long, Y. Li, Y. Chen, X. Chen, S. Zhao, Z. Lin and J. Luo, Non-π-conjugated Deep-Ultraviolet Nonlinear Optical Crystal $K_2Zn_3(SO_4)(HSO_4)_2F_4$, *J. Phys. Chem. Lett.*, 2021, **12**, 8280–8284.
24 X. Xu, C. Hu, F. Kong, J. Zhang, J. Mao and J. Sun, $Cs_2GeB_4O_9$: A New Second-Order Nonlinear-Optical Crystal, *Inorg. Chem.*, 2013, **52**, 5831–5837.
25 Y. Li, Z. Zhou, S. Zhao, F. Liang, Q. Ding, J. Sun, Z. Lin, M. Hong and J. Luo, A Deep-UV Nonlinear Optical Borosulfate with Incommensurate Modulations, *Angew. Chem., Int. Ed.*, 2021, **60**, 11457–11463.
26 C. Huang, M. Mutailipu, F. Zhang, K. J. Griffith, C. Hu, Z. Yang, J. M. Griffin, K. R. Poeppelmeier and S. Pan, Expanding the Chemistry of Borates with Functional $[BO_2]^-$ Anions, *Nat. Commun.*, 2021, 12.
27 T. Ouyang, Y. Shen and S. Zhao, Accurate Design and Synthesis of Nonlinear Optical Crystals Employing $KBe_2BO_3F_2$ as Structural Template, *Chin. J. Struct. Chem.*, 2023, **42**, 100024.
28 C. D. McMillen, J. T. Stritzinger and J. W. Kolis, Two Novel Acentric Borate Fluorides: $M_3B_6O_{11}F_2$ (M = Sr, Ba), *Inorg. Chem.*, 2012, **51**, 3953–3955.
29 J. Bruns, M. Podewitz, K. R. Liedl, O. Janka, R. Pöttgen and H. Huppertz, $Cu[B_2(SO_4)_4]$ and $Cu[B(SO_4)_2(HSO_4)]$–Two Silicate Analogue Borosulfates Differing in their Dimensionality: A Comparative Study of Stability and Acidity, *Angew. Chem., Int. Ed.*, 2018, **57**, 9548–9552.
30 Q. Ding, S. Zhao, L. Li, Y. Shen, P. Shan, Z. Wu, X. Li, Y. Li, S. Liu and J. Luo, Abrupt Structural Transformation in Asymmetric $ABPO_4F$ (A = K, Rb, Cs), *Inorg. Chem.*, 2019, **58**, 1733–1737.
31 B. Wu, C. Hu, R. Tang, F. Mao, J. Feng and J. Mao, Fluoroborophosphates: A Family of Potential Deep Ultraviolet NLO Materials, *Inorg. Chem. Front.*, 2019, **6**, 723–730.
32 M. Mutailipu, M. Zhang, H. Wu, Z. Yang, Y. Shen, J. Sun and S. Pan, $Ba_3Mg_3(BO_3)_3F_3$ Polymorphs with Reversible Phase Transition and High Performances as Ultraviolet Nonlinear Optical Materials, *Nat. Commun.*, 2018, **9**, 3089.
33 S. G. Jantz, M. Dialer, L. Bayarjargal, B. Winkler, L. van Wüllen, F. Pielnhofer, J. Brgoch, R. Weihrich and H. A. Höppe, $Sn[B_2O_3F_2]$-The First Tin Fluorooxoborate as Possible NLO Material, *Adv. Opt. Mater.*, 2018, **6**, 2310407.
34 F. Ding, K. J. Griffith, W. Zhang, S. Cui, C. Zhang, Y. Wang, K. Kamp, H. Yu, P. S. Halasyamani, Z. Yang, S. Pan and K. R. Poeppelmeier, $NaRb_6(B_4O_5(OH)_4)_3(BO_2)$ Featuring Noncentrosymmetry, Chirality, and the Linear Anionic Group BO_2, *J. Am. Chem. Soc.*, 2023, **145**, 4928–4933.
35 G. Shi, Y. Wang, F. Zhan, B. Zhang, R. Yang, X. Hou, S. Pan and K. R. Poeppelmeier, Finding the Next Deep-Ultraviolet Nonlinear Optical Material: $NH_4B_4O_6F$, *J. Am. Chem. Soc.*, 2017, **139**, 10645–10648.
36 H. Cheng, F. Li, Z. Yang and S. Pan, $Na_4B_8O_9F_{10}$: A Deep-Ultraviolet Transparent Nonlinear Optical Fluorooxoborate with Unexpected Short Phase-Matching Wavelength Induced by Optimized Chromatic Dispersion, *Angew. Chem., Int. Ed.*, 2022, **61**, e202115669.
37 L. Xiong, L. Wu and L. Chen, A general principle for DUV NLO materials: π-conjugated confinement enlarges band gap, *Angew. Chem., Int. Ed.*, 2021, **60**, 25063–25067.
38 H. Cheng, X. Li, S. Pan and Z. Yang, Two Hydroxyfluorooxoborates Achieving Deep-ultraviolet Cutoff Edges and Moderate Birefringence by Assembling Multi-anionic Groups, *Chem. – Eur. J.*, 2024, **30**, e202400656.
39 M. Cheng, C. Jin, W. Jin and X. Hou, Target-Oriented Synthesis of Borate Derivatives Featuring Isolated $[B_3O_3]$ Six-Membered Rings as Structural Features, *Inorg. Chem.*, 2023, **62**, 9209–9216.
40 C. Jin, F. Li, B. Cheng, H. Qiu, Z. Yang, S. Pan and M. Mutailipu, Double-Modification Oriented Design of a Deep-UV Birefringent Crystal Functionalized by $B_{12}O_{16}F_4(OH)_4$ Clusters, *Angew. Chem., Int. Ed.*, 2022, **61**, e202203984.
41 C. Jin, H. Zeng, F. Zhang, H. Qiu, Z. Yang, M. Mutailipu and S. Pan, Guanidinium Fluorooxoborates as Efficient Metal-free Short-Wavelength Nonlinear Optical Crystals, *Chem. Mat.*, 2022, **34**, 440–450.
42 S. K. Kurtz and T. T. Perry, A Powder Technique for Evaluation of Nonlinear Optical Materials, *J. Appl. Phys.*, 1968, **39**, 3798–3813.
43 C. Chen, Y. Wu and R. Li, The Anionic Group-Theory of the Non-Linear Optical Effect and its Applications in the Development of New High-Quality NLO Crystals in the Borate Series, *Int. Rev. Phys. Chem.*, 1989, **8**, 65–91.
44 W. Kohn, Nobel Lecture: Electronic Structure of Matter-Wave Functions and Density Functionals, *Rev. Mod. Phys.*, 1999, **71**, 1253–1266.
45 M. C. Payne, M. P. Teter, D. C. Allan, T. A. Arias and J. D. Joannopoulos, Iterative Minimization Techniques for Abinito Total-Energy Calculations–Molecular-Dynamics and Conjugate Gradients, *Rev. Mod. Phys.*, 1992, **64**, 1045–1097.
46 S. J. Clark, M. D. Segall, C. J. Pickard, P. J. Hasnip, M. J. Probert, K. Refson and M. C. Payne, First Principles Methods Using CASTEP, *Z. Kristallogr.*, 2005, **220**, 567–570.
47 J. P. Perdew, K. Burke and M. Ernzerhof, Generalized Gradient Approximation Made Simple, *Phys. Rev. Lett.*, 1997, **78**, 1396.

